Integrated multiple multi-photon imaging and Raman spectroscopy for characterizing structure-constituent correlation of tissues

Jhen-Wei Jhan[1], Wei-Tien Chang[2], Hung-Che Chen and Yu-Tsung Lee[1], Ming-Fang Wu [2], Chung-Hsuan Chen[3], and Ian Liau[1*]

[1]Department of Applied Chemistry and Institute of Molecular Science, National Chiao Tung University, Hsinchu, Taiwan
[2]National Taiwan University Hospital and the Collage of Medicine, National Taiwan University, Taipei, Taiwan
[3]The Genomics Research Center, Academia Sinica, Taipei, Taiwan
**Corresponding author: ianliau@mail.nctu.edu.tw*

Abstract: Histopathological imaging of tissues often requires extensive sample preparation including fixation and staining in order to highlight characteristic alterations associated with diseases. Herein, we report an integrated spectro-microscopy approach based on a combination of multi-modal multi-photon imaging and Raman micro-spectroscopy and demonstrate label-free characterization of the structure-constituent correlation of porcine skin. The multi-modal imaging allows the visualization of dermatological features whereas Raman micro-spectroscopy enables the identification of their 'molecular fingerprints'. By obtaining both structural and molecular-level information of tissue constituents, this integrated approach can offer new insight into the patho-physiological status of tissues.

OCIS codes: (170.3880) Medical and biological imaging; (170.5660) Raman spectroscopy; (170.6935) Tissue characterization; (180.4315) Nonlinear microscopy; (300.6230) Spectroscopy, coherent anti-Stokes Raman scattering

References and links

1. E. Brown, T. McKee, E. diTomaso, A. Pluen, B. Seed, Y. Boucher, and R. K. Jain, "Dynamic imaging of collagen and its modulation in tumors in vivo using second-harmonic generation," Nat. Medicine **9**, 796-800 (2003).
2. M. Strupler, A. M. Pena, M. Hernest, P. L. Tharaux, J. L. Martin, E. Beaurepaire, and M. C. Schanne-Klein, "Second harmonic imaging and scoring of collagen in fibrotic tissues," Opt. Express **15**, 4054-4065 (2007).
3. G. Marchesini, E. Bugianesi, G. Forlani, F. Cerrelli, M. Lenzi, R. Manini, S. Natale, E. Vanni, N. Villanova, N. Melchionda, and M. Rizzetto, "Nonalcoholic fatty liver, steatohepatitis, and the metabolic syndrome," Hepatology **37**, 917-923 (2003).
4. W. R. Zipfel, R. M. Williams, and W. W. Webb, "Nonlinear magic: multiphoton microscopy in the biosciences," Nat. Biotechnol. **21**, 1368-1376 (2003).
5. Y. Fu, H. F. Wang, R. Y. Shi, and J. X. Cheng, "Second harmonic and sum frequency generation imaging of fibrous astroglial filaments in ex vivo spinal tissues," Biophys. J. **92**, 3251-3259 (2007).
6. A. Zumbusch, G. R. Holtom, and X. S. Xie, "Three-dimensional vibrational imaging by coherent anti-Stokes Raman scattering," Phys. Rev. Lett. **82**, 4142-4145 (1999).
7. J. X. Cheng, A. Volkmer, L. D. Book, and X. S. Xie, "An epi-detected coherent anti-stokes raman scattering (E-CARS) microscope with high spectral resolution and high sensitivity," J. Phys. Chem. B **105**, 1277-1280 (2001).
8. N. Dudovich, D. Oron, and Y. Silberberg, "Single-pulse coherently controlled nonlinear Raman spectroscopy and microscopy," Nature **418**, 512-514 (2002).
9. C. L. Evans, E. O. Potma, M. Puoris'haag, D. Cote, C. P. Lin, and X. S. Xie, "Chemical imaging of tissue in vivo with video-rate coherent anti-Stokes Raman scattering microscopy," Proceedings of the National Academy of Sciences of the United States of America **102**, 16807-16812 (2005).
10. H. Kano, and H. Hamaguchi, "In-vivo multi-nonlinear optical imaging of a living cell using a supercontinuum light source generated from a photonic crystal fiber," Opt. Express **14**, 2798-2804 (2006).
11. J. P. Ogilvie, E. Beaurepaire, A. Alexandrou, and M. Joffre, "Fourier-transform coherent anti-Stokes Raman scattering microscopy," Opt. Lett. **31**, 480-482 (2006).

#96211 - $15.00 USD Received 14 May 2008; revised 19 Sep 2008; accepted 24 Sep 2008; published 1 Oct 2008

12. C. Heinrich, C. Meusburger, S. Bernet, and M. Ritsch-Marte, "CARS microscopy in a wide-field geometry with nanosecond pulses," J. Raman Spectrosc. **37**, 675-679 (2006).
13. A. Volkmer, "Vibrational imaging and microspectroscopies based on coherent anti-Stokes Raman scattering microscopy," J. Phys. D-Appl. Phys. **38**, R59-R81 (2005).
14. L. Moreaux, O. Sandre, M. Blanchard-Desce, and J. Mertz, "Membrane imaging by simultaneous second-harmonic generation and two-photon microscopy," Opt. Lett. **25**, 320-322 (2000).
15. J. Sun, T. Shilagard, B. Bell, M. Motamedi, and G. Vargas, "In vivo multimodal nonlinear optical imaging of mucosal tissue," Opt. Express **12**, 2478-2486 (2004).
16. S. M. Zhuo, J. X. Chen, T. S. Luo, D. S. Zou, and J. J. Zhao, "Multimode nonlinear optical imaging of the dermis in ex vivo human skin based on the combination of multichannel mode and Lambda mode," Opt. Express **14**, 7810-7820 (2006).
17. T. B. Huff, Y. Shi, Y. Fu, H. F. Wang, and J. X. Cheng, "Multimodal nonlinear optical microscopy and applications to central nervous system imaging," IEEE J. Sel. Top. Quantum Electron. **14**, 4-9 (2008).
18. L. P. Choo-Smith, H. G. M. Edwards, H. P. Endtz, J. M. Kros, F. Heule, H. Barr, J. S. Robinson, H. A. Bruining, and G. J. Puppels, "Medical applications of Raman spectroscopy: From proof of principle to clinical implementation," Biopolymers **67**, 1-9 (2002).
19. Y. S. Huang, T. Karashima, M. Yamamoto, and H. O. Hamaguchi, "Molecular-level investigation of the structure, transformation, and bioactivity of single living fission yeast cells by time- and space-resolved Raman spectroscopy," Biochemistry **44**, 10009-10019 (2005).
20. A. Zoumi, X. A. Lu, G. S. Kassab, and B. J. Tromberg, "Imaging coronary artery microstructure using second-harmonic and two-photon fluorescence microscopy," Biophysical Journal **87**, 2778-2786 (2004).
21. W. R. Zipfel, R. M. Williams, R. Christie, A. Y. Nikitin, B. T. Hyman, and W. W. Webb, "Live tissue intrinsic emission microscopy using multiphoton-excited native fluorescence and second harmonic generation," Proceedings of the National Academy of Sciences of the United States of America **100**, 7075-7080 (2003).
22. P. J. Campagnola, A. C. Millard, M. Terasaki, P. E. Hoppe, C. J. Malone, and W. A. Mohler, "Three-dimensional high-resolution second-harmonic generation imaging of endogenous structural proteins in biological tissues," Biophys. J. **82**, 493-508 (2002).
23. A. Zoumi, A. Yeh, and B. J. Tromberg, "Imaging cells and extracellular matrix in vivo by using second-harmonic generation and two-photon excited fluorescence," Proceedings of the National Academy of Sciences of the United States of America **99**, 11014-11019 (2002).
24. P. Ducimetiere, J. Richard, and F. Cambien, "The pattern of subcutaneous fat distribution in middle-aged men and the risk of coronary heart disease: the Paris Prospective Study," Int. J. Obes. **10**, 229-240 (1986).
25. M. M. Avram, "Cellulite: a review of its physiology and treatment " J. Cosmetic Laser Therapy **6**, 181-185 (2004).
26. A. J. Singer, and R. A. F. Clark, "Cutaneous Wound Healing," New Engl. J. Med. **341**, 738-746 (1999).

1. Introduction

Many pathological transformations of diseased tissues involve alteration of morphological and chemical characteristics. For example, tumor tissues are typically accompanied with the growth of vessels and collagens [1]; fibrosis of lungs may exhibit extensive modification of extracellular matrix [2]; steatohepatitis is often characterized by inflammation of liver with concurrent fat accumulation in hepatocytes [3]. The ability to visualize these pathological characteristics with definite molecular specificity would greatly assist not only the diagnosis of diseases but also the investigation of the underlying pathogenesis in increased details. Histopathology, the microscopic study of diseased tissues, has long been an indispensable standard technique to identify pathological features. Since the contrast related to specific constituents for tissues visualized under conventional optical microscopes is usually insufficient, histological imaging inevitably involves complex specimen preparation in numerous steps including fixation, processing, embedding, sectioning and staining in order to emphasize and recognize the characteristic components of tissues. Other than tedious processes needed, some histological features in the tissue specimen might be distorted or even entirely lost during these procedures. All these limitations raise a demand to develop a more effective approach that is able to characterize specific pathological features of tissues in a label-free manner.

Multi-photon microscopy that possesses many attractive features such as three-dimensional sectioning, deep penetration and none-destructiveness to samples has long been recognized as a powerful tool for biomedical imaging [4]. Among many modalities of multi-photon microscopy, two-photon excited fluorescence (TPEF) and second-harmonic generation (SHG) microscopy are two widely employed techniques for biomedical applications. Multi-photon imaging based on sum frequency generation (SFG) has also been explored [5].

#96211 - $15.00 USD Received 14 May 2008; revised 19 Sep 2008; accepted 24 Sep 2008; published 1 Oct 2008

Recently, coherent anti-Stokes Raman scattering (CARS) microscopy was introduced [6] and developed [7-12] as a new modality of multi-photon imaging. CARS imaging is based on signals that are intrinsic and specific to particular molecular vibrations, thereby possessing chemical contrast with no need to employ exogenous labeling [13]. Due to different contrast mechanisms and molecular origins involved for each imaging modality, simultaneous acquisition of images based on multiple multi-photon imaging modalities can allow the visualization of various tissue constituents with definite spatial co-localization and improved contrast. Nevertheless, most reported work was limited to two combined modalities because a single laser is used for excitation [2,14-16]. Huff et al. employed two synchronized pulsed lasers and demonstrated tri-modal multi-photon imaging of neurons [17]; however, the TPEF signal was generated by introducing exogenous labels. An integration of CARS, SHG and TPEF imaging based entirely on native constituents of tissues with no need of exogenous labeling has not been demonstrated yet. Moreover, the molecular origins of these nonlinear signals generated from tissue constituents remain relatively unexplored.

Raman spectroscopy, on the other hand, allows the characterization of molecular structures. This capability has been utilized extensively in investigating patho-physiological transformation of tissues and life cycles of single cells [18,19]. For this reason, an implementation of Raman spectroscopy with a multi-photon imaging system is expected to not only help elucidate the molecular origin of the observed multi-photon induced signals, but also consolidate the correlation between the contrasts shown in images with specific tissue constituents.

Here we report a new configuration of spectro-microscopy based on an integration of tri-modal multi-photon imaging (CARS, SHG and TPEF) and Raman spectroscopy, and demonstrate our system on porcine skin by showing dermatological features with great contrast and molecular specificity while with no stains.

2. Experiments

2.1 Apparatus

Figure 1 showed the schematic of our multi-modal spectro-microscopy system. A mode-locked Nd:Vanadate laser (PicoTran, High-Q Laser, Austria) that delivered a stable pulse train (1064 nm, 7 ps, 76 MHz) and a synchronously pumped, frequency-doubled, wavelength-tunable optical parametric oscillator (OPO, Levante, APE, Germany) were employed as excitation. The two pulse trains were merged collinearly with a dichroic mirror, directed to an inverted optical microscope (IX71, Olympus, Japan), and focused with a water immersion objective (UPLSAPO 60X, N.A. 1.2, Olympus, Japan) onto the sample. To properly fill the back aperture of the objective and to take into account its chromatic aberration, the diameters of the two beams were adjusted independently with two sets of telescopes. The power of each beam was independently adjusted with polarization optics comprising a half-wave plate and a polarizer. An optical delay line was employed to match the temporal delay of the two pulse trains. To generate a CARS signal specific to the molecular vibration of the CH_2 stretching mode at 2850 cm^{-1}, the wavelength of the OPO has been set at 816.7 nm throughout this work.

#96211 - $15.00 USD Received 14 May 2008; revised 19 Sep 2008; accepted 24 Sep 2008; published 1 Oct 2008

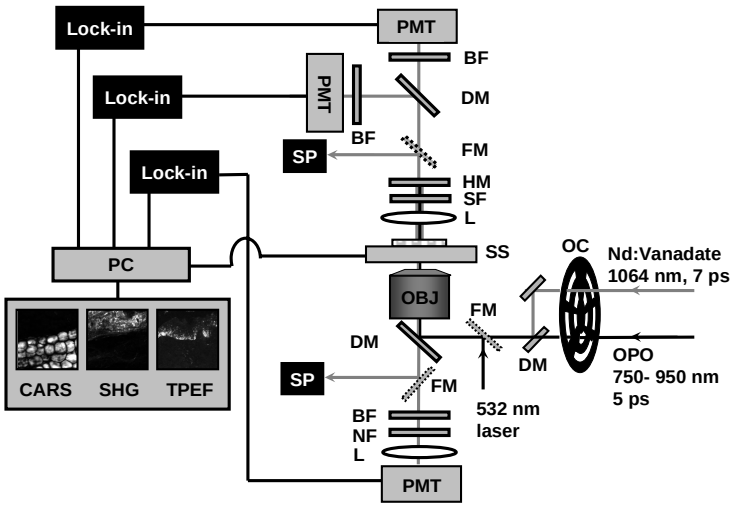

Fig. 1. Schematic diagram of the multi-modal spectro-microscopy system. OC denotes an optical chopper, OBJ a microscope objective, PMT a photomultiplier sensor, SP a spectrograph, BF a bandpass filter, DM a dichroic mirror, FM a 'flipper' mirror, HM a hot mirror, SF a shortpass filter, L a lens, SS a scanning stage, and NF a notch filter.

A microscope condenser lens (N.A. 0.55) was employed to collect signals propagating in the forward direction. The signal passed through a stack of hot mirrors and short-pass filters to block the excitation and was then spectrally split into two directions using a dichroic mirror of a cut-off wavelength at 562 nm. The SHG and CARS signals were further sorted from the split signal beams with a laser-line filter of a center wavelength at 532 nm and with a band-pass filter of a center wavelength at around 660 nm, respectively. The backward-propagating signal was collected with the same objective lens used to focus the excitation. The TPEF signal between 470 and 550 nm was exclusively selected with a band-pass filter by blocking the SHG signal with a notch filter of a center wavelength at 532 nm. The spectrally and spatially separated CARS, SHG and TPEF signals were detected with three photomultiplier sensors (Hamamatsu, Japan). A phase-sensitive detection scheme was also employed to further minimize cross-talk among the three nonlinear signals. The two excitation beams were modulated at two frequencies (typically about 2.3 and 1.9 kHz) with a dual-slot optical chopper (Stanford Research Systems, USA). Each signal was then de-modulated at the corresponding modulation frequency with a lock-in amplifier (Stanford Research Systems, USA). The demodulated signals were then fed to an analog-to-digital converter (National Instruments, USA) and processed with a computer. The scanning of the sample was achieved with a three-axis closed-loop piezo scanning stage (Physik Instruments, Germany). Images were constructed by simultaneously recording the demodulated signals in a point-by-point manner while raster-scanning the sample with respect to the laser focal spot. Throughout this study, the duration time for each pixel was set to 3 ms. An image comprising 300-by-300 pixels typically takes about 4.5 minutes to complete under this setting. Sample scan, signal collection and image construction were implemented with computer codes (LabView, National Instruments, USA). The spatial resolution of our system is 0.37 μm that has determined from the FWHM (full with at half maximum) of a lateral scan on a polymer bead (data not shown).

Spontaneous Raman scattering was generated with a single-frequency, diode-pumped, solid-state laser (532 nm, DPSS Lasers, USA) of which the beam was introduced to the microscope with a 'flipper' mirror. Both the Raman spectra and the multi-photon induced-emission spectra were analyzed with a fiber-coupled spectrograph equipped with a thermoelectrically cooled, charge-coupled device (Shamrock, Andor, USA).

#96211 - $15.00 USD Received 14 May 2008; revised 19 Sep 2008; accepted 24 Sep 2008; published 1 Oct 2008

2.2 Sample preparation

Porcine skin was obtained from domestic pigs slaughtered on the day of the experiment. For multi-modality multi-photon imaging, a thin piece of specimen (~ 1 mm in thickness) was excised from the middle of a pig's ear with a scalpel, placed on a chambered coverslip, immersed in a normal saline solution, and finally sealed with another piece of coverslip directly before imaging.

For histological examination, we employed standard haematoxylin and eosin (H/E) stain on sectioned porcine skin tissue. For collagen and elastin staining, protocols based on Masson's Trichrome and Weigert's methods were used, respectively. Images of stained specimens were acquired with an optical microscope equipped with a digital camera. The results were compared with the multi-modality multi-photon images obtained on untreated specimens.

The scalded skin was prepared by heating the specimens at 60 ^{o}C. The specimens were then examined at different stages (1, 6 and 20 minutes) of thermal injury with the multi-modality multi-photon microscopy.

3. Results and discussion

3.1 Intrinsic multi-photon induced emission from tissue constituents

We first characterized the multi-photon induced emission produced with temporally and spatially overlapped beams of light at 816.7 and 1064 nm. A representative emission spectrum obtained from porcine skin was shown in Fig. 2(A). There are four distinct and sharp spectral lines (centered at 408.4, 462, 532 and 663 nm, respectively) superimposed on a relatively weak but broad spectral band. These four sharp lines were assigned to the SHG (408.4 and 532 nm), SFG (462 nm) and CARS (663 nm) whereas the broad spectral band was attributed to the TPEF in accordance with their corresponding energy-level diagrams that were illustrated in Fig. 2(B). The co-existence of signals from multiple multi-photon processes indicates the co-localization of various tissue components within even a sub-micrometer region as defined by the excitation zone of multi-photon excitation. This complex emission spectrum is not unique to porcine skin; rather, we found it rather common in tissues of various kinds (data not shown).

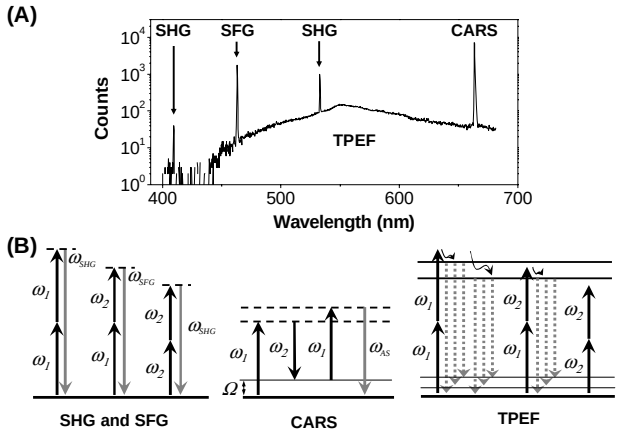

Fig. 2. (A). A representative multi-photon emission spectrum of porcine skin generated using two spatially and temporally overlapped pulsed light sources with λ_1 = 816.7 nm and λ_2 = 1064 nm. The four sharp spectral lines were resulted from SHG (408.4 and 532 nm), SFG (462 nm), and CARS (663 nm), respectively, whereas the broad spectral feature on which the four sharp lines are superimposed was from the TPEF. (B) Energy diagrams corresponding to multiple non-linear optical processes (SHG, SFG, CARS, and TPEF). ω_1 and ω_2 denote two excitation frequencies; ω_{SHG} and ω_{SFG} denote SHG and SFG frequencies; Ω denotes the resonant frequency of a molecular vibration; ω_{AS} denotes the CARS frequency.

#96211 - $15.00 USD Received 14 May 2008; revised 19 Sep 2008; accepted 24 Sep 2008; published 1 Oct 2008

An essential step for the construction of multi-modal multi-photon images and the interpretation of images is to separate signals from individual nonlinear optical processes with minimum cross-talk among them. This is by no means trivial especially for the highly congestive emission spectrum shown in Fig. 2(A). In particular, each coherent signal (i.e. SHG, SFG and CARS) is spectrally overlapped with the TPEF signal. Therefore, it is difficult to separate these signals based only on spectral filtering that has been commonly employed in multi-modal imaging systems. Evan *et al.* reported the utilization of a condenser lens in their CARS microscope to collect forward propagating CARS signals with a good efficiency [9]. We employed also a condenser with a small N.A. to collect coherent signals (SHG, SFG, and CARS) that all propagate in a directional manner while discriminating against incoherent TPEF signals that is, in contrast, divergent. The detection of the fluorescence signal in the forward direction was further attenuated by adjusting the focus of the condenser lens such that only the highly directional beam was effectively focused onto the detectors but not the divergent fluorescence signal. Figure 3 displayed the forward- and backward-collected emission spectra generated from the same focal point of porcine skin. The results clearly showed that the fluorescence was virtually eliminated in the forward-collected spectrum but was largely preserved in the backward direction.

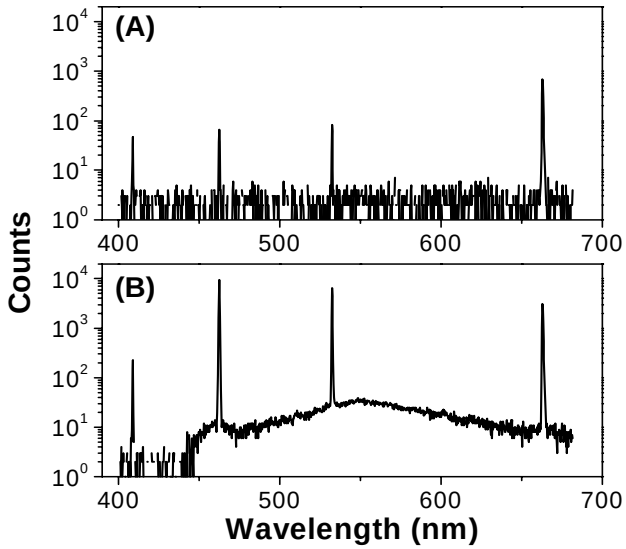

Fig. 3. Comparison of forward- (A) and backward- (B) collected multi-photon induced emission generated at the same focal point (excitation wavelengths: λ_1 = 816.7 nm and λ_2 = 1064 nm).

Although the phase-matching condition favors a propagation of coherent signals in the forward direction, the highly scattering nature of tissues could cause considerable reflection of the coherent signals and result in strong SHG, SFG and CARS signals observed in the backward direction [5]. Despite of this, the TPEF signal can easily be selected without cross-talk using a proper filter set as discussed in the experimental section. Throughout this work, all SHG and CARS images were constructed from signals collected in the forward direction whereas the TPEF images were constructed from that collected in the backward direction, respectively.

3.2 Multi-modality, multi-photon imaging and Raman micro-spectroscopy of porcine skin

Skin is the largest organ that serves as an interface between an animal (or human) body and its surroundings. It also plays an essential role in various physiological functions such as

#96211 - $15.00 USD Received 14 May 2008; revised 19 Sep 2008; accepted 24 Sep 2008; published 1 Oct 2008

regulating body temperature and protecting the body from the invasion of pathogens. Porcine skin shares many common features with human skin in terms of the dermatological structures, and has therefore been commonly utilized as a model system for skin research. It comprises, from the uppermost, the epidermis, dermis and subcutaneous layer. Figure 4(A) showed a cartoon that illustrated a vertical cross section of the skin. The outermost portion of the epidermis is a stratified squamous epithelium whereas the innermost portion of the epidermis is a basal layer with cells that are able to proliferate and to migrate towards the skin surface to replace dead cells. The dermis is separated from the epidermis by a thin laminar layer comprising mainly elastin fibers. The dermis layer has a scattered distribution of cells. These cells are surrounded by extracellular matrix comprising mainly collagen fibers that are arranged in a three-dimensional network. Elastin fibers also exist in the dermis, but their content is relatively small compared to collagen fibers. The most pronounced feature in the subcutaneous layer is adipocytes (fat cells) that are deposited in the pockets of connective tissues serving as an insulating layer to avoid the loss of heat from the skin. We demonstrated label-free visualization of these dermatological features by imaging freshly excised porcine skin without employing stains. Figure 4(B) showed the simultaneously obtained TPEF, SHG and CARS images on separate regions of epidermis, dermis and subcutaneous layers, respectively, whereas Fig. 4(C) displayed the overlaid images in which the signal from each individual nonlinear optical process was coded in a separate color.

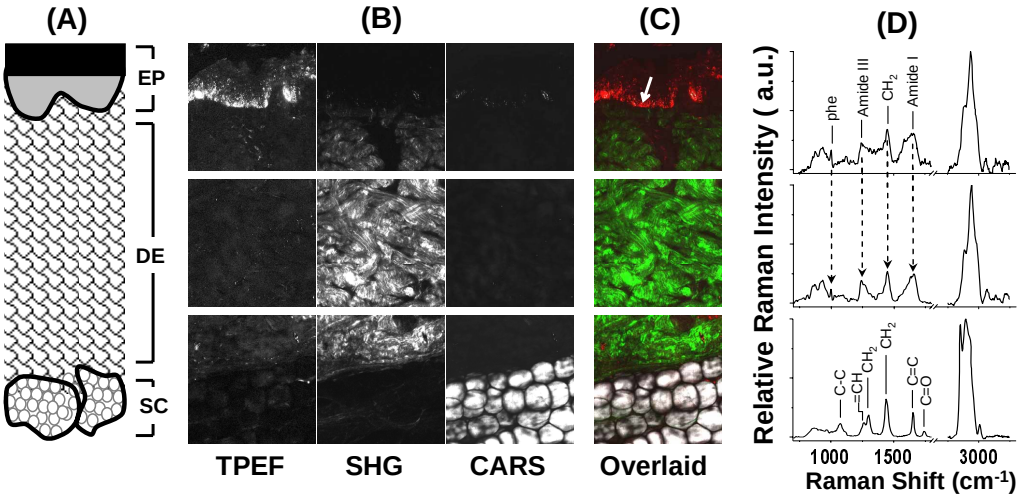

Fig. 4. (A). Cartoon illustration of the cross section of skin. EP denotes the epidermis, DE the dermis, and SC the subcutaneous layer. (B). Simultaneously obtained multi-modal images of the epidermis (upper panel), the dermis (middle panel) and the subcutaneous layer (lower panel) of porcine skin. Scan area: 300 μm x 300 μm; step size: 1 μm. (C). Overlaid multi-modal images produced by coding individual TPEF, SHG and CARS images in red, green and white, respectively. (D). Local Raman spectra measured at regions that exhibited strong TPEF (upper panel), SHG (middle panel) and CARS (lower panel) signals. Excitation wavelength: 532 nm.

We collected TPEF signals in the spectral range between 470 and 550 nm with the contribution from the SHG rejected with a notch filter. The TPEF images showed that the TPEF signal was observed in regions spanning from the epidermis through the dermis. In particular, an area near the epidermis produced strong TPEF signal in the selected spectral range and displayed like a boundary (white arrow). The contribution of the observed TPEF signals might result from natively fluorescent structural proteins and metabolites. Elastin has been reported to produce strong fluorescence about 500 nm [20]. The fluorescence of retinol and NADH also locates within the same spectral window and may also contribute the observed signal [21]. Instead, the contribution from the fluorescence of collagen is small relative to its SHG contribution and can thus be eliminated [20].

#96211 - $15.00 USD Received 14 May 2008; revised 19 Sep 2008; accepted 24 Sep 2008; published 1 Oct 2008

To elucidate the molecular origin of the observed TPEF signals, we measured a Raman spectrum in regions that produced strong TPEF signal and a typical result was shown in the upper panel of Fig. 4(D). The amide I mode (1659 cm^{-1}), amide III mode (1242 cm^{-1}) and the ring-breathing mode of phenylalanine (1004 cm^{-1}) have been observed in the spectrum; all are characteristic vibrational modes of protein molecules. The remaining Raman lines are relatively less specific, but the vibrational line at 1450 cm^{-1} assigned to the bending mode of CH_2, and the unresolved multiple lines near 2900 cm^{-1} assigned to the stretching modes of CH_2 and CH_3 functional groups are also consistent with the vibrational features of proteins. The observation of the vibrational signature of proteins in regions that exhibited strong TPEF signals strongly suggests that the contrast shown in the TPEF image represents mainly the distribution of elastin protein, a natively fluorescent structural protein. Accordingly, the boundary like feature observed in the TPEF image (indicated by the white arrow in Fig. 4(C)) was interpreted as the lamina layer that is known to comprise mainly elastin and locate between the epidermis and dermis layers. The scarce but observable features possessing a characteristic fibrous appearance in the dermis are also consistent with the distribution of elastin in the dermis layer as a constituent of the connective tissue. The result showed that the integration of Raman spectroscopy with multi-modal multi-photon microscopy can facilitate the interpretation of features observed in the images, and also well demonstrated a unique capability in correlating structure-constituent relationship of tissues.

The SHG image was produced from the forward-propagating signal centered at 532 nm. As shown in Figs. 4(B) and (C), strong SHG signal was observed in the dermis layer and the images displayed as a three-dimensional network of fiber bundles that crossed each other, resulting in a pattern similar to densely interwoven meshwork. Many investigators have reported that collagens produce strong SHG signals due to their large second-order polarizability and their non-centrosymmetric structure [1,22,23]. Since collagen is a major component of the extracellular matrix in connective tissues including the dermis layer of skin, the contrast observed in the SHG image was thus attributed to the distribution of collagen fibers. Again, correlated Raman spectral measurement enabled the molecular-level identification of the feature shown in the image based on their 'Raman fingerprints'. As shown in the middle panel of Fig. 4(D), a Raman spectrum measured in a region exhibiting strong SHG signals possessed all characteristic protein lines at 1004, 1246 and 1658 cm^{-1} and consolidated the correlation of the SHG signal to the collagen fibers.

The CARS images were generated from forward propagating signals centered at 663 nm. Strong intensities were only observed in the subcutaneous layer. The images showed many characteristic globular bloated shapes. These features resembled the distribution of adipocytes (fat cells) that mainly locate in the subcutaneous layer. As triglyceride and cholesterol contain many CH_2 functional groups and are the main content of fat, the selection of the excitation wavelengths at 1064 nm and 816.7 nm led to the generation of CARS signals mainly from fat [9]. The feature in the CARS image was thus attributed to the distribution of fat. The correlated Raman spectrum was shown in the lower panel of Fig. 4(D). The spectrum exhibited characteristic Raman lines associated with fat including the C=C stretching (1651 cm^{-1}), the =CH bending (1263 cm^{-1}) and the carbonyl stretching (1740 cm^{-1}) modes of cholesterol and/or triglyceride, and thus supported the attribution of the contrast in the CARS images to adipocyte fat.

In order to visualize various tissue constituents in each demonological layer of skin, we performed a large-area scan (0.3 mm by 3.6 mm) on the porcine skin and the result was displayed in Fig. 5. These images covered regions from the epidermis, dermis, to subcutaneous layer of skin. In particular, the overlaid image exhibited a remarkable contrast, clearly illustrating not only the relative amount but also the spatial distribution of individual tissue constituents in each layer.

#96211 - $15.00 USD Received 14 May 2008; revised 19 Sep 2008; accepted 24 Sep 2008; published 1 Oct 2008

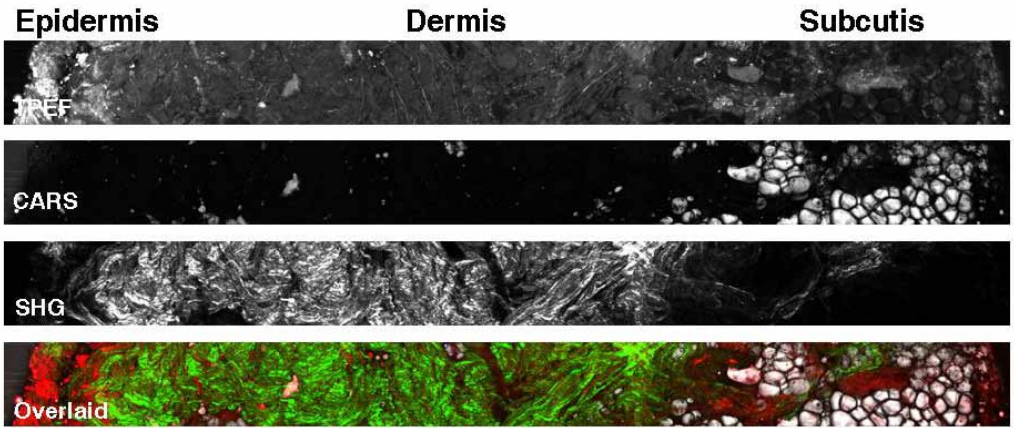

Fig. 5. Large-area, sectional visualization of porcine skin from the epidermis, dermis, to the subcutaneous layer (dimensions: 3.6 mm x 0.3 mm; step size: 1 μm; false colors, green - SHG, red – TPEF, and white - CARS).

Traditional histological imaging requires staining of sectioned specimens in order to selectively highlight particular tissue constituents. We have demonstrated that our multi-modal spectro-imaging system can reveal detailed dermatological features of porcine skin while eliminating the lengthy procedures such as fixation sectioning and staining. We have also shown that the integrated spectroscopic measurement can facilitate the assignments of the characteristic features observed in the multi-modal multi-photon images. To consolidate these points, we compared the histological images of conventional staining with the label-free multi-photon images. The images of conventional staining were shown in Fig. 6.

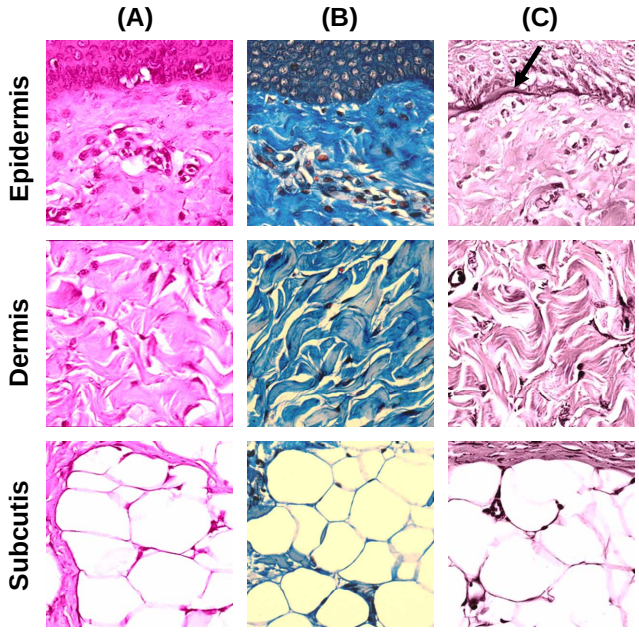

Fig. 6. Histological features of porcine skin highlighted by conventional methods of staining. The images of the H/E stain (A) showed distinct morphological features on the epidermis, dermis, and the subcutis. The images of collagen (B) and elastin (B) stain exhibited bluish and dark purple colors for collagen and elastin, respectively. The laminar layer stained in dark purple was highlighted by an arrow. Image area: 300 μm x 300 μm

#96211 - $15.00 USD Received 14 May 2008; revised 19 Sep 2008; accepted 24 Sep 2008; published 1 Oct 2008

H/E stain is the most commonly used method for the histological diagnosis of diseases. It involves the utilization of basophilic and acidic dyes to color tissue components and produce contrast seen under optical microscopes. Figure 6(A) displayed the H/E stain images obtained in different regions of the porcine skin. These images exhibited distinctly different morphological features in the epidermis, dermis, and subcutis. In particular, the characteristic fibrous bundles in the dermis, and the empty vacuoles in the subcutaneous layer were all well recognized. There features were assigned to collagen and fat, respectively. Although the assignment of these components has been well documented in the literature, H/E stain is relatively lack of specificity to particular tissue constituents. Therefore, special stains are usually required in order to confirm the existence of a particular tissue component of interest.

Masson's Trichrome stains that selectively color collagen in blue are frequently used to identify collagen in tissues. As seen in Fig. 6(B), blue colored fibers were observed in the dermis; a result indicates the abundance of collagen fibers in the dermis and supports the interpretation of the SHG images shown in Fig. 4(B). Weigert's stain was employed to demonstrate elastin fibers and the result was displayed in Fig. 6(C). Again, the thin dark purple line observed between the epidermis and dermis was also consistent with the assignment of the TPEF features shown in the multi-photon image to the elastin constituent in the lamina layer.

Similar to conventional staining, the overlaid multi-photon images can well demonstrate characteristic dermatological features of the porcine skin. Specifically, elastin, collagen, and fat droplets can all be selectively visualized based on their intrinsic nonlinear optical signals, with no need of introducing special stains. This multiple multi-photon imaging can potentially be applied in a variety of clinical or research fields to bring more insight to the patho-physiological status of tissues. To demonstrate its potential clinical applications, we used a scald porcine skin that was subjected to different extents of thermal injury, and examined the dynamic changes along the pathogenic process. Figure 7 showed the results obtained on the same specimen after accumulative heating at 60 ^{o}C for 1, 6, and 30 min, respectively.

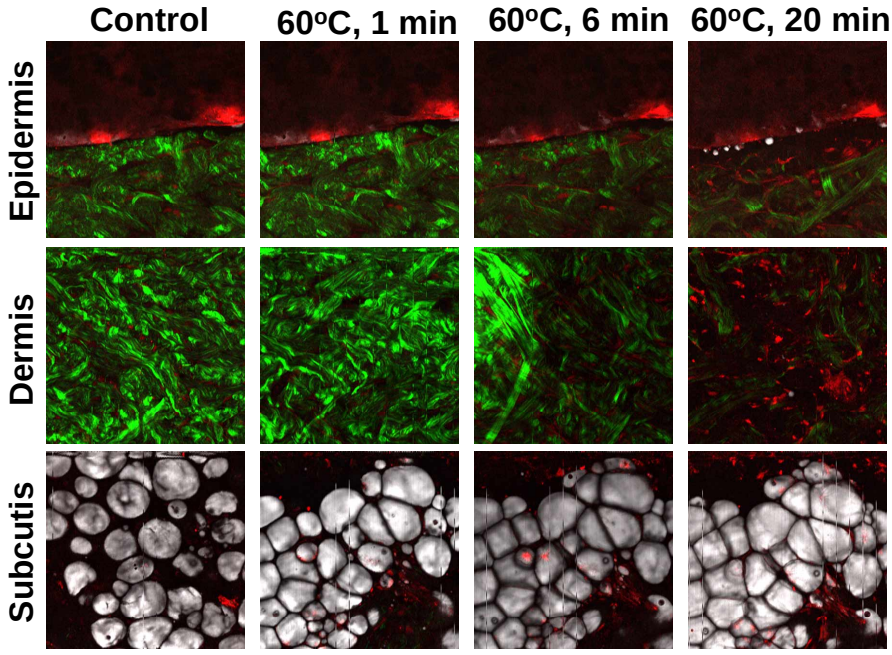

Fig. 7. Overlaid multi-modal images showing the histological change of porcine skin subjected to different extents of scalding. Scan area: 300 µm x 300 µm; step size: 0.5 µm. False colors: green - SHG, red – TPEF, and white - CARS.

#96211 - $15.00 USD Received 14 May 2008; revised 19 Sep 2008; accepted 24 Sep 2008; published 1 Oct 2008

Along the heating process, the TPEF signal showed no significant change, with strong fluorescence preserved in the laminar layer. The fat droplets in the subcutaneous region appeared to enlarge during the heating process. This may result from the deformation of fat droplets or the confluence of small droplets into large ones during heating. The most significant change was the drastic decrease of the SHG intensity in the dermis layer. The reduced SHG intensity from collagen may result from denature of collagens during the heating process.

The result shown above is of great clinical interest. In contrast to traditional histological examination that requires laborious specimen processing, our approach allows immediate illustration of detailed histological or pathological changes on intact tissues without the need of fixation, sectioning and stains. Most remarkably, the dynamic changes in response to repeated or accumulative physical or chemical injuries can be sequentially imaged on the same area, thereby eliminating the concerns of possible artifacts introduced by the preparation processes.

This approach can also be extended to investigate the pathology of other diseases. Specifically, the image may serve as an indicator for the risks of other systemic diseases. For example, the distribution of subcutaneous fat has been recognized as a risk factor for coronary heart diseases [24]. An excessive accumulation of subcutaneous fat has also been suggested to precede cellulite, a condition describing the alteration of the topography of skin [25]. Besides, wound healing is a dynamic recovering process involving considerable alterations in the component and structure of skin [26]; during the remodeling phase of wound healing, the collagen fibers begin to consolidate, and the relation between collagen and elastin in the dermal region alters. All these features can potentially be visualized with chemical specificity by this multi-modal spectro-microscopy approach. In particular, the ability to visualize the structures of multiple tissue constituents and to characterize these constituents with molecular details provides a means to monitor the alteration of tissues associated with diseases and to evaluate the outcome of therapeutic interventions that are being investigated.

4. Summary

We report an integrated multi-modal, spectro-microscopy approach that allows chemically specific, high-resolution, multi-modal, non-linear imaging and spectroscopic measurements on the same region of unstained tissues. We demonstrated the visualization of detailed histological features of porcine skin without introducing stains and also discussed the potential applications of this multi-modal, multi-photon spectro-microscopy system for label-free tissue imaging.

Acknowledgments

We thank Yuan-Pern Lee and John Ogilvie for comments on the manuscript. We are also grateful to Yuan-Pern Lee, Kien-Wen Sun and Jeng-Tzong Sheu for the use of their equipment, and Chao-Yu Chung and Hung-Lung Lin for technical assistance. National Science Council and the MOE-ATU program of Taiwan provide support to Ian Liau.

#96211 - $15.00 USD Received 14 May 2008; revised 19 Sep 2008; accepted 24 Sep 2008; published 1 Oct 2008